Electronic transport properties in graphene oxide frameworks

P. Zhu,[1] E. Cruz-Silva,[1,2] and V. Meunier[1,*]

[1]*Department of Physics, Applied Physics, and Astronomy, Rensselaer Polytechnic Institute, Troy, New York 12180, USA*

[2]*Department of Polymer Science and Engineering, University of Massachusetts, Amherst, Massachusetts 01003 USA*

(Received 20 September 2013; revised manuscript received 2 February 2014; published 28 February 2014)

The electronic transport properties in multiterminal graphene oxide framework (GOF) materials are investigated using a combination of theoretical and computational methods. GOFs make up four-terminal ⌆-shaped GNR-*L*-GNR junctions where sandwiched boronic acid molecules (*L*) are covalently linked to two graphene nanoribbons (GNRs) of different edge chiralities. The transport properties are governed by both tunneling and quasiresonant regimes. We determine how the presence of linker molecules affects the transport properties and establish that the through-molecule transport properties can be tuned by varying the chemical composition of the pillar molecules but are not significantly modified when changing the type of electrodes from zigzag GNRs to armchair GNRs. In addition, we find that in multilinker systems containing two parallel molecules in the device area, the coupling between the molecules can lead to both constructive and destructive quantum interferences. We also examine the inability of the classical Kirchhoff's superposition law to account for electron flow in multilinker GOF nanonetworks.

DOI: 10.1103/PhysRevB.89.085427 PACS number(s): 73.63.−b, 73.23.Ad, 84.30.Bv

I. INTRODUCTION

Electron transport in molecular junctions is an active and promising research area which is enjoying sustained activities from experiment, theory, and nanodevice fabrication fields. Over the last decade, substantial work in experiments and theoretical simulations focused on electronic transport properties in a variety of different molecules for traditional metal-molecule-metal junctions such as break junctions and electron-migration junctions [1–8]. Developing an atomistic-level understanding of the processes responsible for a junction's response to a specific external stimulus is drawing increasing attention, with the clear goal of devising nanoelectronic applications approaching the atomic-level miniaturization size limit in functional devices [9]. Traditional metal-molecule-metal junctions consist of a single molecule or a group of a few molecules stretched between macroscopic metallic electrodes where the coupling between the molecule and the macroscopic electrodes significantly influences the electron transport properties of the junction. However, this coupling is hard to fully characterize given the vast range of possible configurations at the interface. Typically, the usually weak coupling significantly limits the transport properties of the junctions, as shown in a number of experiments [10–12]. The problem is worsened by inherent material stochasticity and poorly defined metal-molecule contacts, as evidenced by the variability in reported results obtained using state-of-the-art experimental techniques. It follows that the reliability and reproducibility of a metal-molecule-metal junction remains a wide open research problem for the development of molecular electronics [8,13–16]. To overcome the difficulties associated with the metal-molecule coupling uncertainty, new electrode material candidates such as graphene, graphene nanoribbons (GNRs), and silicon nanowires have been proposed [17–22] as they can provide a better-defined electrode-molecule contact via covalent bonds. Covalent bonds are interesting not only because of their coupling strength but also because of the directionality of the bonding they allow, which significantly reduces uncertainty and variability, compared to weakly bonding interactions such as van der Waals forces.

GNRs are promising electrode materials and are currently favored as ideal candidates for building blocks for all-carbon-based nanoelectronics due to their unusual electronic and transport properties, as well as the availability of increasingly precise fabrication techniques [22–25]. However, turning to molecular junctions, it remains difficult to imagine how break junctions or even lithographically assembled junctions could benefit from the use of GNR electrodes, especially for bulk production. Indeed, the control over the open-edge properties of GNRs is still a vast work in progress, and a full understanding is still lacking as far as the atomic details of interfacial properties at the edges of GNRs are concerned [26–29]. Here we explore alternative opportunities emerging from recent developments in low-dimensional multicomponent system synthesis. Specifically, a viable alternative to well-defined GNR/molecule interfaces has been developed in the context of layered molecular frameworks such as graphene oxide frameworks (GOFs). GOFs are made up of stacked graphene sheets covalently bonded by boronic acid pillar units positioned perpendicular to the carbon plane. They were first synthesized using graphene oxide sheets (GO) and linker boronic acid in a solvothermal reaction during which strong B-O bonds are formed between boronic acids and oxygen functional groups on the GO layers [30,31]. Chemical reduction can then be used to remove unreacted oxygen functional groups on GO layers. Previous theoretical work demonstrated that GOFs possess a range of possible electronic properties that can be tuned by a proper selection of linker size and density [32]. Inspired by the experimental feasibility of the junctions and their predicted properties, we propose here an original setup for a class of four-terminal GNR-*L*-GNR junctions, where a single or group of boronic acid molecules *L* covalently connect two parallel GNRs, which are themselves seamlessly connected to GNR electrodes, thereby forming a four-terminal ⌆ -shaped junction.

*meuniv@rpi.edu; http://homepages.rpi.edu/~meuniv/

We focus here on model junctions generically referred to as GNR-(B)PDBA-GNR. An example of such a junction is shown in Fig. 1(a), where the sandwiched molecule is a 1,4-phenyldiboronic acid (PDBA $\equiv L$) that links two GNRs of zigzag edge chirality. Examples using a longer linker [4,4′-biphenyldiboronic acid (BPDBA $\equiv L'$)] and armchair GNR electrodes were also considered. The choice of systems enables a study of the effect of varying the composition and the number of the pillaring molecules as well as the type of GNR electrodes. Our objective is to show that the molecular junctions synthesized in bulk in the fabrication of GOFs show promise for the development of scalable bottom-up nanoelectronics where functional devices with reproducible properties can be built from the interplay between properties of graphene layers and single-molecule junctions. We also explore how structural and electronic factors affect electronic transport in molecular junctions and at the same time improve the existing understanding of quantum interference effects responsible for departures from the classical Kirchhoff's superposition law (KSL) in molecular transport junctions. To achieve these goals, we use density functional theory (DFT) and the Landauer-Büttiker formalism for multiprobe transport calculations.

This paper is organized as follows. In Sec. II, we present the technical details related to the methods used for transport calculations. In Sec. III, the computational results are presented and discussed for several junction models which can be classified by the type of electrodes into two kinds: zGNR-L-zGNR junctions which use zigzag GNRs (zGNRs) as electrodes and aGNR-L-aGNR junctions which use armchair GNRs (aGNRs). Discussion and concluding remarks are presented in Secs. IV and V.

II. METHODS

All the electronic transport calculations were performed using DFT [33,34] combined with the equilibrium Green's-function formalism specifically developed for transport in multiterminal nanojunctions [35,36]. The DFT portion of the work used the SIESTA code [37] in the generalized gradient approximation (GGA) with the Perdew-Burke-Ernzerhof (PBE) exchange-correlation functional [38]. The wave functions were expanded in a double-ζ basis set with polarization. The finite-range numerical pseudoatomic orbitals used an energy shift of 50 meV [39]. The Brillouin zone was sampled with a Monkhorst-Pack grid [40] corresponding to four nonequivalent k points in the ribbon growth direction. A real-space mesh is used to compute integrals over potential and charge and with numerical parameters equivalent to a plane-wave cutoff energy of 250 Ry.

A zigzag GNR with eight atoms along the width direction (8-zGNR) and an armchair GNR with nine atoms along the width direction (9-aGNR) were considered as electrodes. Fifteen and eleven unit cells constituted one slice of 8-zGNR and 9-aGNR, respectively. The edges of both ribbons were passivated with a single hydrogen atom per edge carbon site to increase thermodynamic stability [41]. In addition, we also explored dihydrogenated aGNRs, where each edge carbon atom is passivated with two hydrogen atoms, since recently published works revealed that this could be a more stable configuration for armchair edges under standard conditions (nonzero temperature and nonzero hydrogen concentrations) [26,42]. A minimum vacuum distance of 11 Å was maintained between supercells in the GNR's finite-size directions to avoid interactions with images in the nonperiodic directions. All models were relaxed by conjugate gradient minimization until the maximum force was less than 0.04 eV/Å. For all the systems considered, an electrode used for transport calculations was made up of either three zGNR or two aGNR unit cells on each end of the systems.

The transport and density of states (DOS) calculations were performed using an in-house transport code based on the Landauer-Büttiker formalism outlined by Datta [43] and used in previous similar studies [25,44,45], using the converged Hamiltonian and overlap matrices from SIESTA to build the Green's functions. We present two types of DOS plots. The first type corresponds to a density of states averaged over the atoms of a unit cell of the electrode, far from the active device region. The second type averages states over all the atoms of the active region in contact with the electrodes. Both spin-up and spin-down polarized transport calculations were performed for the systems involving zGNR electrodes, while non-spin-polarized calculations were performed in the aGNR cases.

III. RESULTS

We first study the properties of the model structure shown in Fig. 1(a). The operative details of the methodology adopted for transport calculations will be illustrated in reference to this particular model. For the DFT calculations, the system is explicitly treated as periodic in the transport direction and is divided into five parts: top left lead, top right lead, bottom left lead, bottom right lead, and active device region (D) indicated by thick lines. The electrodes are semi-infinitely extended within the framework of surface Green's-function formalism. In this example, the D region consists of a single PDBA molecule linker and a portion of the nearby parts of GNRs to include the molecule-GNR interaction. This is done in such a way that the virtual junction between the device region and the electrode is sufficiently far away from the active part of the actual covalent junction to minimize spurious interface effects. In this study, the aGNR-based electrodes were treated in their ground, nonmagnetic state. In contrast, for each zGNR electrode, we adopted an antiferromagnetic configuration across opposite mono-hydrogen-passivated edges since it corresponds to the ground state [23]. Spin-polarized transport calculations show that the parallel or antiparallel relative spin alignments between the top zGNR electrode and the bottom zGNR electrode cause no significant difference in the transmission functions (not shown). Since no spin-dependent transport was observed, we will only discuss transmission functions for spin-up polarization. The quantum conductance plots shown throughout this paper are based on the transmission coefficients $T_{i\to j}(E)$ between any two electrodes i and j of the junctions. Hereafter we use the symbol T_{GG} (graphene-graphene) to represent transmission coefficients for transmission pathways that do not explicitly include a molecule. Conversely, T_{GMG} (graphene-molecule-graphene) refers to the pathways that explicitly include a molecule.

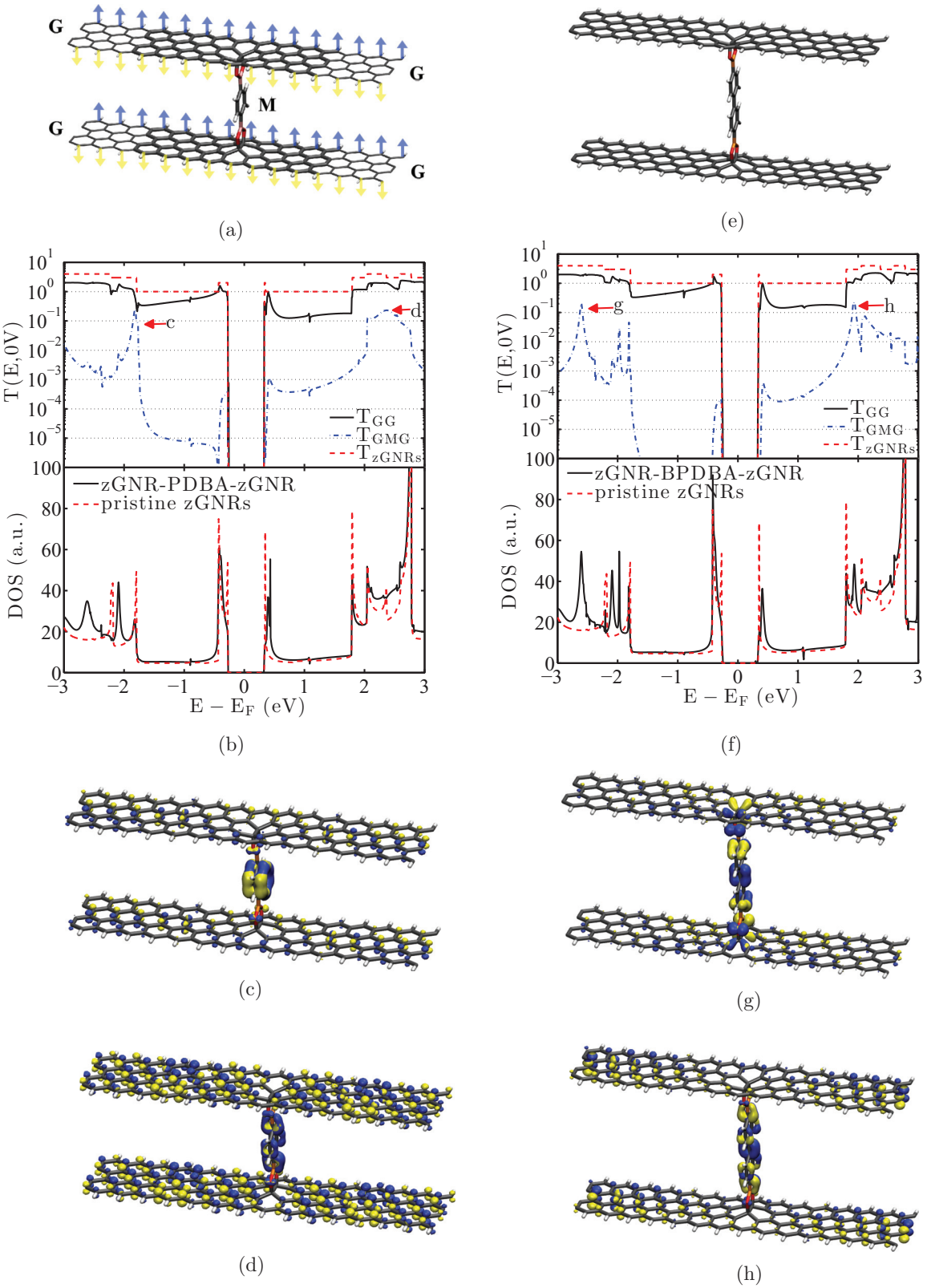

FIG. 1. (Color online) (a) Optimized atomic structure of a four-terminal zGNR-L-zGNR junction ($L \equiv$ PDBA) in the AFM spin configuration for zGNR electrodes. For all the atomic structures discussed in this paper, carbon is shown in gray, boron in orange, oxygen in red, and hydrogen in white and (b) its transmission functions and density of states plots, compared with pristine zGNRs values (dashed red lines). The arrows mark the energy ranges of the charge-density calculations in (c) and (d). (c) and (d) Junction's spin-up (blue) and spin-down (yellow) charge density within the energy ranges $[-1.93, -1.76]$ and $[2.22, 2.52]$ eV. (e) Atomic structure of the zGNR-L'-zGNR junction ($L' \equiv$ BPDBA) and (f) its transmission functions and density of states plots. (g) and (h) Spin-up (blue) and spin-down (yellow) charge density within the energy ranges $[-2.64, -2.57]$ and $[1.89, 1.98]$ eV.

While the four-terminal junctions present two separate GG pathways and four distinct GMG pathways [Fig. 1(a)], we represent only one transmission function for each group since the transmission functions are quasidegenerate within each group.

As expected, the transmission functions are zero in the energy range ± 0.3 eV around E_F corresponding to the gap of the zGNRs electrodes [46] since these have no carriers that can scatter at such energy values [Fig. 1(b)]. Compared to T_{GG}, T_{GMG} has two clear peaks indicated by letters c and d in Fig. 1(b) in the energy ranges $[-1.93, -1.76]$ and [2.22,2.52] eV. The local charge density integrated within these ranges and plotted in Figs. 1(c) and 1(d) provides an understanding of the origin of these two peaks: they are characterized by enhanced distributions of states significantly localized on the linker molecule. The transmission is therefore resonant with a quasimolecular state of the linker, which accounts for the boost in resonant transmission along the GMG pathway. At those energies, the transmission across the linker is almost as large as that for the GG path, indicating that the junction can be used as a current divider.

Experimentally, boronic acid linkers can be chosen in various lengths. To address this possibility, we consider the BPDBA as connecting unit which differs from PDBA by the presence of an additional phenyl ring in its structure, and will be represented as L' hereafter. Figure 1(e) shows the corresponding zGNR-L'-zGNR junction. When the transport through the molecule is nonresonant, the corresponding transmission is expected to be reduced since a longer molecule causes a higher barrier for electron tunneling according to the elastic scattering mechanism [47]. As expected, the calculated $T(E)$ in Fig. 1(f) does show such a reduction: comparing $T^{L'}_{GMG}$ in Fig. 1(f) with T^{L}_{GMG} in Fig. 1(b), the BPDBA junction displays a $\sim$21% reduction for the through-molecule conductance when compared to the PDBA case. In contrast, quasiresonance occurs for the specific energy values indicated by arrows labeled with the letters g and h in Fig. 1(f). The local charge density plots of Figs. 1(g) and 1(h) were calculated within the energy ranges $[-2.64, -2.57]$ and [1.89,1.98] eV around the peak values, revealing that the peaks in $T^{L'}_{GMG}$ are linked to the presence of localized states on the linker BPDBA molecule within those energy ranges. However, for non-through-molecule pathways (T_{GG}), the two junctions studied up to now share very similar transmission functions because the local structure around the linker is not significantly modified by the change in linker type.

The results presented thus far have been limited to molecular junctions comprised of a single linker molecule. We now consider the effect of multiple linkers. The results will be contrasted later with results expected within the framework of the classical Kirchhoff's superposition law (KSL). In a purely classical system, KSL states that the conductance of an electronic circuit made up of two individual branches prepared in a parallel configuration is equal to the sum of the conductance of these two branches ($G_{tot} = G_1 + G_2$). The main assumptions are that individual resistances are not affected by the presence of the others and that the connecting wires are resistance free. However, for a molecular-scale circuit, this classical law is not likely to be valid since the electronic transport is dominated by quantum physics, and nontrivial behavior is expected to emerge from the interplay between properties of individual components of the device region [48]. The quantum interference effects for two parallel branches in a molecular circuit can be either constructive or destructive depending on energy, and it is therefore not expected that KSL can even provide a limiting value in nanoscale systems. To illustrate the inadequacy of using KSL in GOF-based circuits, we first investigated three possible parallel configurations based on zGNR-LL-zGNR junctions with various separation distances d_{LL} between the two molecules [Figs. 2(a), 2(e), and 2(i)]. The three systems contain two PDBA molecules in parallel in the device region, with separation distances d_{LL} varying from 1 to 3 in units of the length of a zGNR unit. The corresponding transmission functions are plotted in Figs. 2(b), 2(f), and 2(j).

Before examining the GMG transmission pathways, we first discuss the in-plane transmission T_{GG} corresponding to pathways that do not explicitly involve transmitting through the molecule. The most obvious differences in T_{GG} between the zGNR-LL-zGNR junctions and the zGNR-L-zGNR junction [Figs. 2(b), 2(f), and 2(j) vs Fig. 1(b)] are the emergence of peaks highlighted by arrows labeled c,h,k, and l in Figs. 2(b), 2(f), and 2(j). Further, we observe the emergence of valleys in T_{GG} marked by blue arrows labeled d and g in Figs. 2(b) and 2(f), indicating that T_{GG} at those energy ranges are suppressed by the interference induced by the presence of the two parallel molecules. To better understand the origin of these features, local charge density integrated around the energy indicated by these arrows is plotted in Figs. 2(c), 2(d), 2(g), 2(h), 2(k), and 2(l). The isosurface plots show that the peaks in T_{GG} are due to constructive quantum interference in the region between the molecules, which leads to a significant increase in transmission. In contrast, the suppressed transmissions at the energy ranges marked by the blue arrows are likewise accounted for by destructive quantum interference, which causes a node in the wave function on the graphene material between the molecules [Figs. 2(d) and 2(g)], thus effectively shutting off transmission and explaining the large suppression of conductance along the GG pathways. The coexistence of both constructive and destructive quantum interferences due to the two parallel PDBA molecules reveals the level of complexity we can expect in the behavior of conductance in multilinker systems. In fact, the behavior of electrons in the double-linker configuration is reminiscent of the well-known phenomenon of electronic interference in a double-slit experiment, where each molecular linker plays the role of a slit.

To further compare our findings to the results of an analysis based on the KSL, we compared the through-molecule transmission of zGNR-LL-zGNR systems (T^{LL}_{GMG}) with two times the through-molecule transmission of zGNR-L-zGNR systems ($2T^{L}_{GMG}$) [49]. The presence of peaks and zeros in the T^{LL}_{GMG} functions that are absent in T^{L}_{GMG} immediately confirms the inability of Kirchhoff's law to account for the GOF conductance. For instance, in the zGNR-LL-zGNR ($d_{LL} = 2$ zGNR units) vs zGNR-L-zGNR case, T^{LL}_{GMG} are estimated to be 60 times larger than $2T^{L}_{GMG}$ at the energy point indicated by the black arrow labeled h in Fig. 2(f). The origin of these peaks and valleys can be traced back to constructive and destructive quantum interferences in the local charge density of the unbiased system, as shown in Figs. 2(c), 2(d), 2(g), 2(h), 2(k), and 2(l).

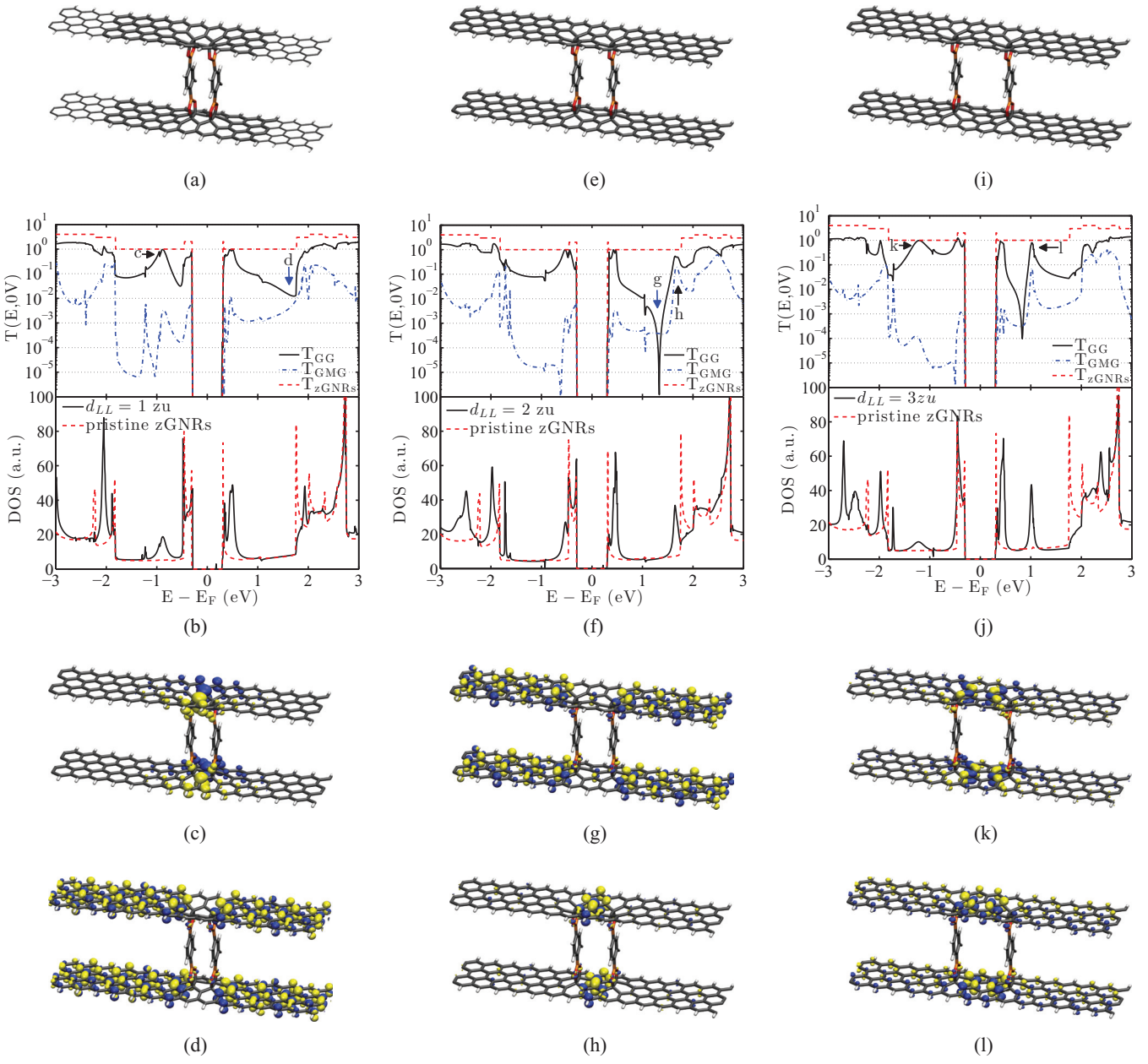

FIG. 2. (Color online) (a)/(e)/(i) Atomic structure of the zGNR-LL-zGNR junction ($d_{LL} = 1/2/3$ zGNR units). d_{LL} represents the separation distance between the two molecules. (b)/(f)/(j) Transmission functions and density of states plots for the $d_{LL} = 1/2/3$ zGNR unit systems, compared with pristine zGNR values (dashed red lines). $T(E)$ at the energy ranges indicated by the black arrows labeled c,h,k,l exhibit constructive quantum interference while those indicated by the blue arrows labeled d,g exhibit destructive quantum interference. (c)–(d)/(g)–(h)/(k)–(l) Partial charge density within the energy ranges $[-1.03, -0.73]$ and $[1.22,1.72]/[1.17,1.47]$ and $[1.57,1.77]/[-1.43, -1.03]$ and $[0.92,1.12]$ eV.

Another case of interest is that instead of changing the chemical composition or the number of the linker molecules, we can also alter the type of GNR electrodes. Thus, we now examine the effect of replacing the zGNR electrodes by aGNR ones on the overall transmission behavior [Fig. 3(a)]. Compared to the previously studied case, the PDBA molecule is rotated by 90°, as this orientation satisfies the lattice constraints while at the same time preserving the system symmetry. The wider energy gap in the electronic structure of aGNRs [46] results in a wider conductance gap around E_F for aGNR-L-aGNR when compared to the zGNR case. The aGNR junction also has larger transmission amplitudes for the T_{GG} pathways, with similar amplitudes for the T_{GMG} pathways in the energy range of [2.22, 2.52] eV. This result indicates the limited influence of changing electrodes from zGNRs to aGNRs on the transmission functions for through-molecule pathways. This is particularly true in the present case where the linker is attached fairly far from the edge since the transmission is then governed by valley states rather than edge states, which unlike the former, are significantly affected by edged chirality. Similar to the origin of the peaks in T_{GMG} of the zGNR-L-zGNR junction [Fig. 1(d)], the peak in T_{GMG} of the aGNR-L-aGNR

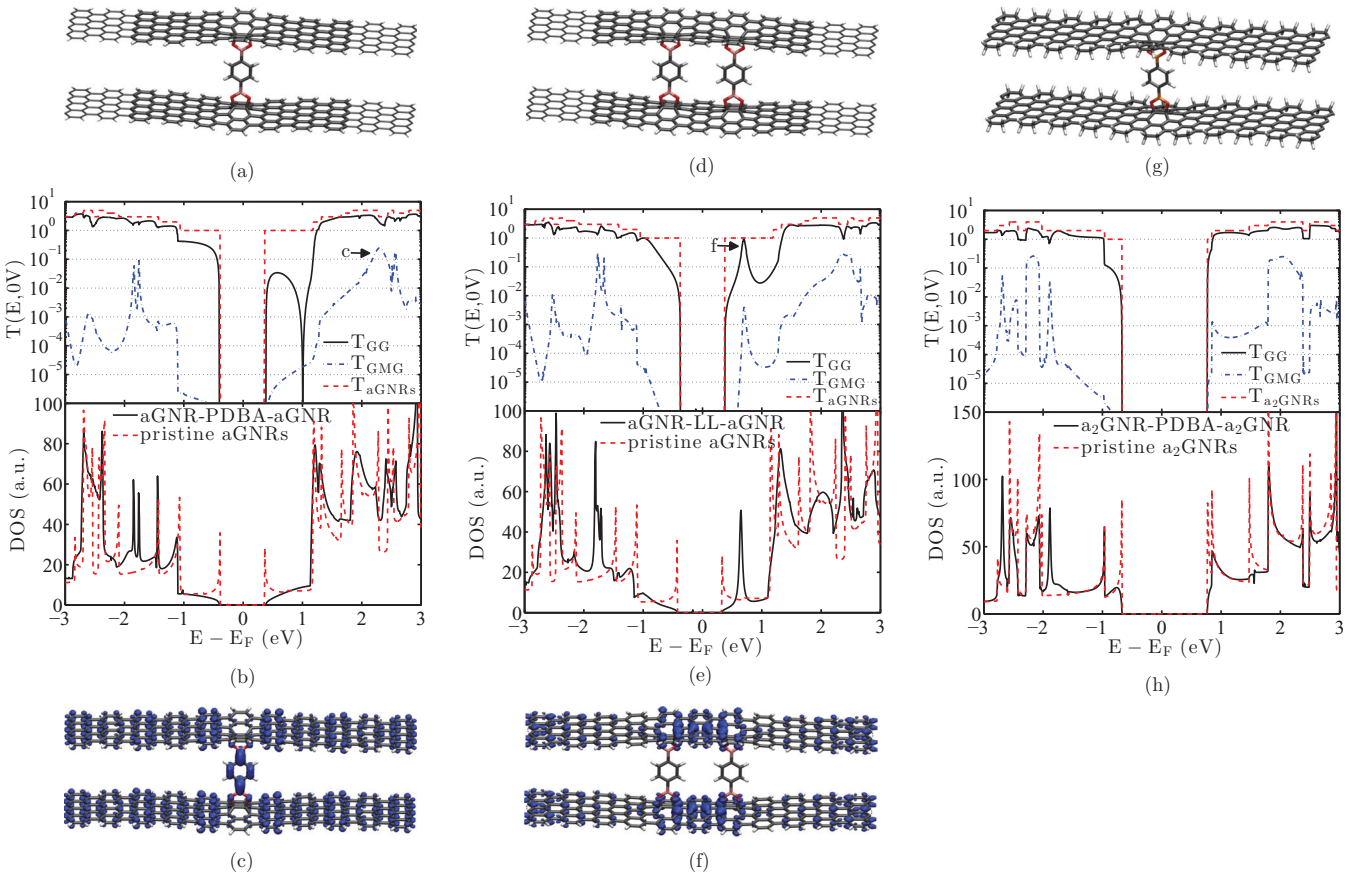

FIG. 3. (Color online) (a) Atomic structure of the aGNR-L-aGNR junction ($L \equiv$PDBA) and (b) corresponding transmission functions and density of states plots, compared with pristine aGNRs values (dashed red lines). (c) Partial charge density integrated over the energy range [2.18, 2.42] eV. (d) Structure of the aGNR-LL-aGNR junction. (e) Transmission functions and density of states plots. (f) Partial charge density within the energy range [0.56, 0.86] eV. (g) Atomic structure of the a_2GNR-LL-a_2GNR junction. a_2GNR represents armchair graphene nanoribbons with dihydrogenated edges. (h) Its transmission functions and density of states plots, compared with pristine a_2GNR values (dashed red lines).

junction is due to resonance with quasimolecular states located on the linker molecule as shown in Fig. 3(c), which have a spatial distribution very similar to that of the zGNR-L-zGNR junction. The results also show that the transport properties of the through-molecule pathways are largely dictated by the local bonding and the intrinsic properties of the linker.

Starting from the aGNR-L-aGNR junction, we constructed an aGNR-LL-aGNR junction with two PDBA molecules in parallel in the device region and separated by a distance of 2 aGNR units. The separation distance was chosen to minimize van der Waals interactions between the two molecule linkers and at the same time to prevent the perturbation of the electrodes' Hamiltonian due to the conducting linkers (the closer the linkers are to the electrodes, the larger the perturbation is expected to be). We find the presence of a peak of conductance indicated by the arrow labeled f when examining the difference in T_{GG} between the aGNR-LL-aGNR and the aGNR-L-aGNR junctions [Fig. 3(e) vs Fig. 3(b)]. Note that this peak also corresponds to a peak in the DOS plot, thereby revealing the presence of localized states. This is confirmed by examining the partial charge density within the energy range [0.56, 0.86] eV around the peak energy [Fig. 3(f)], which highlights the emergence of a charge distribution compatible with constructive quantum interference due to the coupling between the molecules [49].

In many theoretical studies, zigzag and armchair edges, as the two achiral edge geometries of graphene nanoribbons, are usually saturated with a single hydrogen per edge carbon atom site to achieve stability, as done in the results shown up to now. However, a number of recent theoretical works have revealed that armchair edges terminated with two hydrogens are possibly a more thermodynamically stable configuration under standard conditions (nonzero temperature and nonzero hydrogen concentration). To establish the effect of edge termination on the transmission in GOF-based junctions, we have therefore also considered an aGNR-PDBA-aGNR junction where the aGNR electrodes have dihydrogenated edges and have calculated its transmission properties [Figs. 3(g) and 3(h)]. Here armchair graphene nanoribbons are denoted as a_iGNRs, where i stands for the number of hydrogen atoms per edge carbon site. Our calculation shows that the transmission functions of an a_2GNR-PDBA-a_2GNR junction, compared to that of an a_1GNR-PDBA-a_1GNR junction [Fig. 3(h) vs Fig. 3(b)], have a much wider gap around E_F (∼1.4 eV) and a somewhat smaller amplitude for T_{GG} at most energy values, while they have a minor difference for T_{GMG}. The

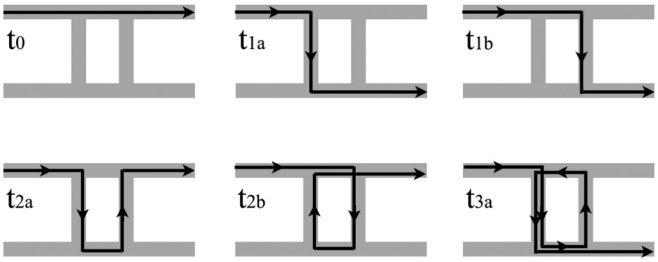

FIG. 4. Diagrammatic representations of the leading Feynman transmission paths for multilinker system. Only one possible t_3 is shown.

limited influence of altering the aGNR's termination on T_{GMG} again confirms the conclusion that these through-molecule transmission functions are mainly determined by the local C-O bonding and the intrinsic properties of the linker PDBA molecule.

IV. DISCUSSION

We conclude the study of multilinker systems with a discussion of the transmission using the concept of Feynman path analysis (Fig. 4). It should be stressed that because of the presence of two linkers, $T_{\mathrm{GG}}(E)$ not only includes the explicit GNR-to-GNR transmission t_0 but is also influenced by Feynman paths of higher orders [47]. For example, the second-order path $t_{2a,b}$ corresponds to electrons transmitting from one GNR through a linker and then back to the GNR through the other linker. The Landauer formalism implicitly accounts for the Feynman paths at all orders [47]. Within this context, the applicability of KSL can be further assessed by testing whether the properties of the multilinker system can be understood solely on the basis of the properties of a single-linker system. Due to the geometry of the GOF structure and neglecting interferences between transmission pathways (i.e., working at lowest order), the path GMG of two-linker systems can be seen as the *parallel* combination of two GMG elements of one-linker systems ($t_{1a} \parallel t_{1b}$). Using similar conditions, the second-order path GG of two-linker systems (t_{2a}, for example) consists of the *serial* combination of two GMG elements of a one-linker system. It is interesting to note that from a Feynman path analysis, the GMG pathway corresponds to odd-numbered passages through any linker, while the GG pathway entices transmission through even-numbered (including zero) linkers. For instance, at first order, the GMG pathway corresponds to two parallel one-linker circuits (t_{1a}, t_{1b}), while at second order, the GG pathway corresponds to two parallel two-linker-in-series circuits (t_{2a}, t_{2b}). Third-order pathways include multiple three-linker-in-series circuits such as t_{3a}. However, because the overall electronic properties of the assembly are not a simple superposition of the properties of the individual systems, the transmission properties cannot be expressed in terms of single-linker properties.

V. CONCLUSIONS

Compared with traditional metal-molecule-metal junctions, GOF-based GNR-L-GNR junctions present the advantages of well-defined geometry and strong covalent coupling between the GNR electrodes and organic molecules. Our results reveal that both structural and electronic factors affect electronic transport properties of GNR-L-GNR and GNR-LL-GNR junctions and at the same time enhance the understanding of quantum interference effects in molecular electronics. For single-linker systems, T^{L}_{GMG} is essentially determined by the local bonding and the intrinsic properties of the linker molecule and therefore shows both tunneling and quasiresonant behaviors. The transmission function T_{GMG} changes with the length of the linker but is only slightly affected by changing the electrode type from zGNR to aGNR, provided molecules are anchored at a distance from the edges of the nanoribbon. In contrast, T^{L}_{GG} is not affected by the length of the pillaring units since the in-plane transport is only modified by local sp^3 bonding at the anchoring point. For multilinker systems, transport behavior is significantly more complicated with the existence of both constructive and destructive quantum interferences due to the coupling between the two parallel linker molecules. The presence of peaks and valleys in the T^{LL}_{GMG} and T^{LL}_{GG} functions that are absent in T^{L}_{GMG} and T^{L}_{GG} implies the inability of Kirchhoff's law to account for the conductance. It follows that the transport in multipillar systems cannot be understood from the sole knowledge of the transport in single-pillar structures. While in this paper we only focus on GNR-L-GNR junctions that have a symmetric structure, fixed zGNR or aGNR widths, and fixed molecule orientation, more research should be performed to explore the transport properties of GNR-L-GNR junctions with heterogeneous GNR structures and altering molecule positions/orientations.

ACKNOWLEDGMENTS

This work was supported by New York State under NYSTAR Contract No. C080117 and by the Office of Naval Research. Computations were performed ar Rensselaer Polytechnic Institute's CCI.

[1] K. Moth-Poulsen and T. Bjørnholm, Nat. Nanotechnol. **4**, 551 (2009).
[2] J. Park, A. N. Pasupathy, J. I. Goldsmith, C. Chang, Y. Yaish, J. R. Petta, M. Rinkoski, J. P. Sethna, H. D. Abruña, P. L. McEuen *et al.*, Nature (London) **417**, 722 (2002).
[3] J. J. Parks, A. R. Champagne, G. R. Hutchison, S. Flores-Torres, H. D. Abruña, and D. C. Ralph, Phys. Rev. Lett. **99**, 026601 (2007).
[4] T. Taychatanapat, K. I. Bolotin, F. Kuemmeth, and D. C. Ralph, Nano Lett. **7**, 652 (2007).
[5] M. A. Reed, C. Zhou, C. Muller, T. Burgin, and J. Tour, Science **278**, 252 (1997).
[6] S. Y. Quek, L. Venkataraman, H. J. Choi, S. G. Louie, M. S. Hybertsen, and J. B. Neaton, Nano Lett. **7**, 3477 (2007).
[7] J. G. Kushmerick, D. B. Holt, J. C. Yang, J. Naciri, M. H. Moore, and R. Shashidhar, Phys. Rev. Lett. **89**, 086802 (2002).

[8] B. Kim, S. H. Choi, X.-Y. Zhu, and C. D. Frisbie, J. Am. Chem. Soc. **133**, 19864 (2011).
[9] N. Tao, Nat. Nanotechnol. **1**, 173 (2006).
[10] A. Nitzan and M. A. Ratner, Science **300**, 1384 (2003).
[11] P. D. Williams and M. G. Reuter, J. Phys. Chem. C **117**, 5937 (2013).
[12] M. G. Reuter, M. C. Hersam, T. Seideman, and M. A. Ratner, Nano Lett. **12**, 2243 (2012).
[13] L. Venkataraman, J. E. Klare, C. Nuckolls, M. S. Hybertsen, and M. L. Steigerwald, Nature (London) **442**, 904 (2006).
[14] H. Basch, R. Cohen, and M. A. Ratner, Nano Lett. **5**, 1668 (2005).
[15] S.-H. Ke, W. Yang, and H. U. Baranger, Nano Lett. **8**, 3257 (2008).
[16] H. Basch and M. Ratner, J. Chem. Phys. **119**, 11926 (2003).
[17] P. Avouris, Z. Chen, and V. Perebeinos, Nat. Nanotechnol. **2**, 605 (2007).
[18] E. C. Girão, A. G. S. Filho, and V. Meunier, Nanotechnology **22**, 075701 (2011).
[19] S.-H. Ke, H. U. Baranger, and W. Yang, Phys. Rev. Lett. **99**, 146802 (2007).
[20] W. Lu, V. Meunier, and J. Bernholc, Phys. Rev. Lett. **95**, 206805 (2005).
[21] N. P. Guisinger, M. E. Greene, R. Basu, A. S. Baluch, and M. C. Hersam, Nano Lett. **4**, 55 (2004).
[22] M. Terrones, A. R. Botello-Méndez, J. Campos-Delgado, F. López-Urías, Y. I. Vega-Cantú, F. J. Rodríguez-Macías, A. L. Elías, E. Muñoz-Sandoval, A. G. Cano-Márquez, J.-C. Charlier *et al*., Nano Today **5**, 351 (2010).
[23] L. Pisani, J. A. Chan, B. Montanari, and N. M. Harrison, Phys. Rev. B **75**, 064418 (2007).
[24] E. Cruz-Silva, Z. M. Barnett, B. G. Sumpter, and V. Meunier, Phys. Rev. B **83**, 155445 (2011).
[25] E. C. Girão, E. Cruz-Silva, and V. Meunier, ACS Nano **6**, 6483 (2012).
[26] C. K. Gan and D. J. Srolovitz, Phys. Rev. B **81**, 125445 (2010).
[27] C. Tao, L. Jiao, O. V. Yazyev, Y.-C. Chen, J. Feng, X. Zhang, R. B. Capaz, J. M. Tour, A. Zettl, S. G. Louie *et al*., Nat. Phys. **7**, 616 (2011).
[28] G. Xie, Z. Shi, R. Yang, D. Liu, W. Yang, M. Cheng, D. Wang, D. Shi, and G. Zhang, Nano Lett. **12**, 4642 (2012).
[29] M. Pan, E. C. Girão, X. Jia, S. Bhaviripudi, Q. Li, J. Kong, V. Meunier, and M. S. Dresselhaus, Nano Lett. **12**, 1928 (2012).
[30] J. W. Burress, S. Gadipelli, J. Ford, J. M. Simmons, W. Zhou, and T. Yildirim, Angew. Chem. Int. Ed. **49**, 8902 (2010).
[31] G. Srinivas, J. W. Burress, J. Ford, and T. Yildirim, J. Mater. Chem. **21**, 11323 (2011).
[32] P. Zhu, B. G. Sumpter, and V. Meunier, J. Phys. Chem. C **117**, 8276 (2013).
[33] P. Hohenberg and W. Kohn, Phys. Rev. **136**, B864 (1964).
[34] W. Kohn and L. J. Sham, Phys. Rev. **140**, A1133 (1965).
[35] K. K. Saha, W. Lu, J. Bernholc, and V. Meunier, J. Chem. Phys. **131**, 164105 (2009).
[36] E. C. Girão, G. Souza Filho, and V. Meunier, Appl. Phys. Lett. **98**, 112111 (2011).
[37] J. M. Soler, E. Artacho, J. D. Gale, A. García, J. Junquera, P. Ordejón, and D. Sánchez-Portal, J. Phys. Condens. Matter **14**, 2745 (2002).
[38] J. P. Perdew, K. Burke, and M. Ernzerhof, Phys. Rev. Lett. **77**, 3865 (1996).
[39] J. Junquera, Ó. Paz, D. Sánchez-Portal, and E. Artacho, Phys. Rev. B **64**, 235111 (2001).
[40] H. J. Monkhorst and J. D. Pack, Phys. Rev. B **13**, 5188 (1976).
[41] V. Barone, O. Hod, and G. E. Scuseria, Nano Lett. **6**, 2748 (2006).
[42] T. Wassmann, A. P. Seitsonen, A. M. Saitta, M. Lazzeri, and F. Mauri, Phys. Rev. Lett. **101**, 096402 (2008).
[43] S. Datta, *Quantum Transport: Atom to Transistor* (Cambridge University Press, Cambridge, 2005).
[44] V. Meunier and B. G. Sumpter, J. Chem. Phys. **123**, 024705 (2005).
[45] A. R. Botello-Méndez, E. Cruz-Silva, J. M. Romo-Herrera, F. López-Urías, M. Terrones, B. G. Sumpter, H. Terrones, J.-C. Charlier, and V. Meunier, Nano Lett. **11**, 3058 (2011).
[46] Y.-W. Son, M. L. Cohen, and S. G. Louie, Phys. Rev. Lett. **97**, 216803 (2006).
[47] S. Datta, *Electronic Transport in Mesoscopic Systems* (Cambridge University Press, Cambridge, 1997).
[48] C. Joachim, Nat. Nanotechnol. **7**, 620 (2012).
[49] See Supplemental Material at http://link.aps.org/supplemental/10.1103/PhysRevB.89.085427 for a detailed comparison of T_{GMG} for GNR-LL-GNR junctions and GNR-L-GNR junctions.